Proceedings of ICFDP7
SEVENTH INTERNATIONAL CONFERENCE OF FLUID DYNAMICS AND PROPULSION
December 18-20, 2001, Cairo, Egypt

ICFDP7-2001031

ACOUSTIC RADIATION FROM AN ANNULAR CASCADE IN A SWIRLING FLOW

Amr A. Ali *
University of Notre Dame
Notre Dame, IN 46556
Email: aali@nd.edu

Oliver V. Atassi†
Pratt & Whitney
East Hartford, CT 06108
Email: atassio@pweh.com

Hafiz M. Atassi ‡
University of Notre Dame
Notre Dame, IN 46556
Email: atassi@nd.edu

Abstract

The propagation of time-harmonic acoustic waves in a nonuniform swirling mean flow is studied. A second order accurate numerical scheme is used to solve the linearized Euler equations for an annular duct geometry. A three dimensional 'exact' nonreflecting boundary condition is applied downstream of the truncated duct. Numerical solutions are compared with normal mode analysis for validation. As an application, the numerical code is used to study the scattering of a gust by a row of blades. The solutions are compared to those of linearized lifting surface theories. The strip theory approximation for the three dimensional scattering problem is also examined.

INTRODUCTION

Accurately computing the propagation of acoustic and vortical waves in a duct with nonuniform flow is a fundamental component of many aeroacoustic problems. For example in fan interaction noise, wakes periodically shed from a fan interact with downstream lying guide vanes to produce noise. The complete fan interaction noise problem requires modeling the rotor-stator interaction. However, this approach is hindered by mathematical and numerical difficulties as well as by the computational intensiveness of modeling the rotor and stator simultaneously. A common approach is to limit the size of the computational domain and confine the calculations to a single blade row. The mathematical formulation of the single blade row is then treated as a forced response problem where the inlet and/or outlet excitations are imposed, and the scattered field representing both vortical and acoustic waves must be accurately determined. The inlet and outlet boundary conditions, required to complete the boundary-value problem, must be nonreflecting to satisfy the causality condition that energy from the source must propagate out of the computational domain.

The first part of this paper is concerned with the computation of time-harmonic acoustic waves in a duct with nonuniform swirling flow. The numerical difficulties associated with the numerical scheme and the nonreflecting boundary conditions due to the nonuniformities of the flow will be discussed. The results presented in this part form the basis for the direct computation of forced response problems resulting from incident vortical and/or acoustic waves interacting with a blade row. In the second part of the paper we study the forced response problem of a gust scattered by a row of blades. The numerical code will be validated against the semi-analytic results of the lifting surface theories for a uniform mean flow.

For uniform flows, the far-field solutions can be expressed in terms of a superposition of normal modes. By selecting the normal modes corresponding to outgoing waves (based on energy propagation) to represent the scattered field, a normal mode expansion satisfying the causality condition can be constructed. The expansion can then be used to derive an expression for the flow quantities at the inlet (outlet) computational boundary in terms of the flow quantities at a location inside the boundary. This expression, which represents an exact nonreflecting boundary condition, can be truncated for use in computations. In two dimensions with uniform upstream and downstream mean flow, this approach was used by Fang and Atassi [3] to obtain solutions to the generalized wave equation about a cascade of blades and

* Research Assistant, Fellow, Center for Applied Mathematics.
† Research Engineer, Member ASME.
‡ Viola D. Hank Professor, Fellow ASME.

Copyright © 2001 by ASME

by Giles [4] who expanded the primitive variables of the linearized Euler equations in terms of normal modes. In three-dimensions, Atassi [2] used this approach for an annular duct geometry in a uniform mean flow and showed that it suffices to write the non-reflecting condition for the pressure with a pure convection condition for the vortical modes.

For three-dimensional nonuniform mean flows with swirl, the normal mode spectrum consists of a discrete set of pressure-dominated modes and a set of discrete and continuous vorticity dominated modes [7]. Although accurate numerical solutions can be obtained for the pressure-dominated modes , the existence of a singular critical layer for the vortical modes and the localized shape of the convected eigensolutions make it very difficult to obtain accurate numerical solutions for the vorticity-dominated modes. Moreover, the eigenvalue problem resulting from the normal mode analysis is not self-adjoint and, as a result, the normal modes may not form a complete set [6]. Consequently, an accurate representation of general far-field disturbances using only a normal mode representation is questionable.

Even if accurate far-field boundary conditions can be formulated, spurious waves resulting from nonuniform grid spacing or poor grid resolution may reflect at the boundary. This may especially occur in time-dependent or time-periodic problems that start from an arbitrary initial discontinuous state and then march in time until a converged solution is attained. In such cases, the initial condition may introduce a range of wavenumbers and frequencies which may reflect at the boundary even when exact boundary conditions are derived [13].

In the present work, the linearized Euler equations are solved for an annular duct geometry and nonreflecting boundary conditions are derived for disturbances to a nonuniform mean flow with swirl. The boundary conditions use the normal mode analysis presented by Ali et. al. [1] to represent the acoustic modes. The nonreflecting boundary conditions are implemented in a linearized Euler scheme. The Euler scheme starts from an arbitrary initial state and uses pseudo time-marching to converge to a steady state solution. The propagation of acoustic modes in a swirling mean flow in an annular duct is computed and studied. This problem serves as an excellent and quantifiable means of assessing the accuracy of the numerical scheme since the normal mode analysis provides an 'exact' solution with which to measure the accuracy of the results. The numerical code is then used to study the acoustic radiation from an annular cascade interacting with an incident gust. The solutions are compared to those of linearized lifting surface theories of Namba [10] and Schulten [11] for uniform flows. Finally, the strip theory approximation is examined by comparing the three dimensional calculations to a two dimensional calculations based on that theory.

Mathematical Formulation

We assume a non-viscous, non-heat-conducting fluid and use the Euler Equations as the governing equations. The flow quantities are then expanded as follows

$$\mathbf{U}(\mathbf{x},t) = \mathbf{U}_0(\mathbf{x}) + \mathbf{u}(\mathbf{x},t), \tag{1}$$

$$p(\mathbf{x},t) = p_0(\mathbf{x}) + p'(\mathbf{x},t), \tag{2}$$

$$\rho(\mathbf{x},t) = \rho_0(\mathbf{x}) + \rho'(\mathbf{x},t), \tag{3}$$

where $\mathbf{x}$ represents the position vector, $\mathbf{U}_0$, p_0, ρ_0 are the steady mean velocity, pressure, and density, respectively. The corresponding unsteady perturbation quantities, $\mathbf{u}$, p', ρ' are such that $|\mathbf{u}(\mathbf{x},t)| \ll |\mathbf{U}_0(\mathbf{x})|$, $|p'(\mathbf{x},t)| \ll p_0(\mathbf{x})$, and $|\rho'(\mathbf{x},t)| \ll \rho_0(\mathbf{x})$.

The mean flow is assumed axisymmetric and of the form,

$$\mathbf{U}(\mathbf{x}) = U_x(r)\mathbf{e}_x + U_s(r)\mathbf{e}_\theta, \tag{4}$$

where U_x and U_s are the mean velocity components in the axial and circumferential directions, respectively. $\mathbf{e}_x$ and $\mathbf{e}_\theta$ represent unit vectors in the axial and circumferential directions, respectively. The mean flow is, in general, vortical with vorticity given by

$$\vec{\zeta} = \nabla \times \mathbf{U} = \frac{1}{r}\frac{d(rU_s)}{dr}\mathbf{e}_x - \frac{dU_x}{dr}\mathbf{e}_\theta. \tag{5}$$

The stagnation enthalpy, temperature, entropy, velocity, and vorticity are related by Crocco's equation

$$\nabla H = T\nabla S + \mathbf{U} \times \vec{\zeta}. \tag{6}$$

We assume time-harmonic disturbances of the form $e^{-i\omega t}$. Since the numerical scheme used for our computations is explicit, we retain the time derivative terms in the equations with the understanding that they will vanish for large time. The linearized Euler equations can be written as follows,

$$\left([I](\frac{\partial}{\partial t} - i\omega) + [A_x]\frac{\partial}{\partial x} + [B_\theta]\frac{1}{r}\frac{\partial}{\partial \theta} + [C_r]\frac{\partial}{\partial r} + [D]\right)\mathbf{Y} = 0, \tag{7}$$

where

$$\mathbf{Y} = \begin{bmatrix} \rho' \\ u_x \\ u_\theta \\ u_r \end{bmatrix}, \tag{8}$$

Copyright © 2001 by ASME

$$[A_x] = \begin{bmatrix} U_x & \rho_o & 0 & 0 \\ \frac{c_o^2}{\rho_o} & U_x & 0 & 0 \\ 0 & 0 & U_x & 0 \\ 0 & 0 & 0 & U_x \end{bmatrix}, \quad (9)$$

$$[B_\theta] = \begin{bmatrix} U_s & 0 & \rho_o & 0 \\ 0 & U_s & 0 & 0 \\ \frac{c_o^2}{\rho_o} & 0 & U_s & 0 \\ 0 & 0 & 0 & U_s \end{bmatrix}, \quad (10)$$

$$[C_r] = \begin{bmatrix} 0 & 0 & 0 & \rho_o \\ 0 & 0 & 0 & 0 \\ 0 & 0 & 0 & 0 \\ \frac{c_o^2}{\rho_o} & 0 & 0 & 0 \end{bmatrix}, \quad (11)$$

and

$$[D] = \begin{bmatrix} 0 & 0 & 0 & \frac{d\rho_o}{dr} + \frac{\rho_o}{r} \\ 0 & 0 & 0 & \frac{dU_x}{dr} \\ 0 & 0 & 0 & \frac{U_s}{r} + \frac{dU_s}{dr} \\ \frac{d}{dr}(\frac{c_o^2}{\rho_o}) & 0 & \frac{-2U_s}{r} & 0 \end{bmatrix}, \quad (12)$$

where $[I]$ is the unit matrix and u_x, u_θ, and u_r are the components of the disturbance velocity $\mathbf{u}$ in the axial, circumferential, and radial directions, respectively.

For a flow in an annular duct with rigid walls, the impermeability condition must be satisfied giving the following boundary condition at the hub and tip radii,

$$u_r(x,\theta,r_h) = u_r(x,\theta,r_t) = 0. \quad (13)$$

An explicit second order accurate Lax Wendroff scheme is used to solve the pseudo-time form of the 3-D linearized Euler equations. The computational domain is an annular sector of angle θ_e.

Without loss of generality, the upstream disturbance can be written in the form,

$$\mathbf{u_I}(r,\theta) = \sum_{m'=-\infty}^{\infty} \mathbf{a_{m'}}(r) e^{i(m'\theta - \omega t)}, \quad (14)$$

$$\rho_I'(r,\theta) = \sum_{m'=-\infty}^{\infty} A_{m'}(r) e^{i(m'\theta - \omega t)}. \quad (15)$$

Considering one of the above Fourier modes, a quasi-periodic condition is applied in the θ direction,

$$\mathbf{Y}(x,\theta_e,r) = \mathbf{Y}(x,0,r) e^{i\sigma}. \quad (16)$$

In the case of the rotor/stator interaction problem, $\theta_e = \frac{2\pi}{V}$ and $m' = pB$, where p is an integer and B and V are the number of rotor and stator blades, respectively. The interblade phase angle σ is given by,

$$\sigma = m'\theta_e - 2q\pi = \frac{2\pi}{V}(pB - JV), \quad (17)$$

where J is an integer.

Computations are performed using curvilinear coordinates (ξ,η,ζ) which make the computer code flexible and can be used with complex geometries. For the calculations shown in this paper, a uniform grid is used with the ξ lines are chosen to be streamlines. η and ζ lines are lines located in planes of constant x. η lines are lines of constant radius and ζ lines are radial lines at $x = 0$ evolving with the streamlines as x increases.

For simplicity, we model the swirling mean flow component as a combination of a rigid body rotation and a free vortex,

$$U_s = \Omega r + \frac{\Gamma}{r}. \quad (18)$$

This model can be defined by the two constant parameters Ω and Γ. We further assume the flow to be isentropic with a uniform enthalpy from hub to tip. In this case, the axial component of velocity is given by

$$U_x^2 = U_o^2 - 2[\Omega^2(r^2 - r_m^2) + 2\Omega\Gamma\ln(\frac{r}{r_m})], \quad (19)$$

where U_o is the axial velocity at the mean radius of the duct r_m. It is convenient for presenting the numerical results to define the axial and swirl velocities in terms of the Mach numbers at the mean radius $M_0 = U_0/c_{om}$, $M_\Omega = (\Omega r_m)/c_{om}$ and $M_\Gamma = \Gamma/(r_m c_{om})$, where c_{om} is the speed of sound at r_m. We nondimensionalize lengths with respect to the mean radius r_m, and define the reduced frequency as $\frac{\omega r_m}{c_{om}}$.

Nonreflecting Boundary Conditions

Away from the noise source the farfield behavior of the scattered unsteady disturbances is governed by the eigenmode analysis given in a previous paper [1]. The eigenmode analysis showed that the pressure content of the acoustic modes is several order of

Copyright © 2001 by ASME

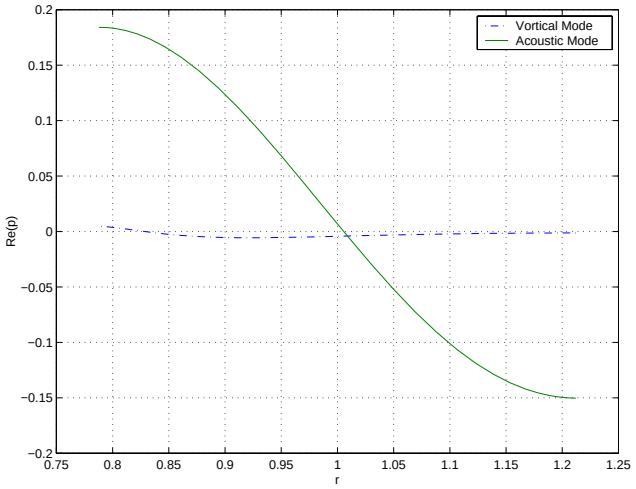

Figure 1. Pressure eigenfunctions of the acoustic eigenmode of the smallest pressure content compared to the vortical eigenmode of the biggest pressure content ($M_o = 0.5$, $M_\Omega = M_\Gamma = 0.2$, and $m = -1$).

magnitudes larger than the pressure content of the vortical modes as shown in Fig. 1. This figure shows the pressure eigenfunction corresponding to one of the vortical modes compared to the pressure eigenfunction corresponding to one of the acoustic modes for a case of $M_o = 0.5$, $M_\Omega = M_\Gamma = 0.2$, $m = -1$, and reduced frequency of 2π. The vortical mode ($k_{-1,3} = 11.7626$) shown in the figure has the biggest pressure content among the vortical modes. The acoustic mode shown in this figure is the second downstream propagating mode ($k_{-1,2} = -2.4639$). Each eigenmode is normalized such that a vector containing the pressure, the axial velocity, the circumferential velocity, and the radial velocity eigenfunctions has a unit norm.

Relying on these results we represent the unsteady pressure or density in the farfield in terms of the acoustic modes,

$$\rho'^{\pm}(r,\theta,x) = \sum_{m=-\infty}^{\infty} \sum_{n\in S_{mn}^{\pm}} c_{mn}^{\pm} P_{mn}^{\pm}(r) e^{i(k_{mn}^{\pm}x + m\theta)}, \qquad (20)$$

where k_{mn} and $P_{mn}(r)$ are the axial wave number and the corresponding density eigenfunction of the mode (mn), respectively. $S_{mn}^{\pm}$ is the set of modes decaying or propagating upstream $(-)$ or downstream $(+)$.

To satisfy the causality condition that energy from the source must propagate out of the computational domain, the $(+)$ modes in equation (20) are considered for the downstream boundary conditions while the $(-)$ modes are considered for the upstream boundary conditions. The direction of propagation is determined using the group velocity, $\frac{d\omega}{dk_{mn}}$, the speed with which the energy propagates [14]. The use of the phase velocity, $\frac{\omega}{k_{mn}}$, may lead to incorrect results especially near the cut-on condition.

For computational purpose we truncate the series of equation (20) to $\tilde{M}$ circumferential modes,

$$\rho'^{\pm}(r,\theta,x) = \sum_{m=-\frac{\tilde{M}}{2}+1}^{\frac{\tilde{M}}{2}} \sum_{n\in\tilde{S}_{mn}^{\pm}} c_{mn}^{\pm} P_{mn}^{\pm}(r) e^{i(k_{mn}^{\pm}x + m\theta)}, \qquad (21)$$

where $\tilde{S}_{mn}^{\pm}$ is a finite subset of $S_{mn}^{\pm}$.

The coefficients c_{mn} are unknown. By using the normal mode expansion at two adjacent planes at the boundary, c_{mn} can be eliminated yielding a nonreflecting boundary condition.

Numerically, let ρ'_{ij} be the value of ρ' at the grid point (i,j) at the exit boundary corresponding to $x = x_N$, where i is the index along the radial direction and j is the index along the circumferential direction,

$$\rho'_{ij} = \sum_{m=-\frac{\tilde{M}}{2}+1}^{\frac{\tilde{M}}{2}} \sum_{n\in\tilde{S}_{mn}^{+}} c_{mn}^{+} P_{mn}^{+}(r_i) e^{i(k_{mn}^{+}x_N + m\theta_j)}. \qquad (22)$$

This can be cast in matrix form,

$$\mathbf{P}_N = [C_N]\mathbf{c}, \qquad (23)$$

where the elements of the vector $\mathbf{P}_N$ are the unsteady density of the different grid points at the exit plane at $x = x_N$. The elements of the vector $\mathbf{c}$ are the coefficients c_{mn}^{+}, and the elements of the matrix $[C_N]$ are the values of the normal modes $P_{mn}^{+}(r_i)e^{i(k_{mn}^{+}x_N + m\theta_j)}$ at (i,j). Note that the number of modes used in the expansion may be smaller than the number of grid points of the computational domain.

Similarly, we can write the solution at the previous axial cross-section located at $x = x_{N-1}$ as,

$$\mathbf{P}_{N-1} = [C_{N-1}]\mathbf{c}. \qquad (24)$$

Solving the previous equation for $\mathbf{c}$,

$$\mathbf{c} = [C_{N-1}]^{-1}\mathbf{P}_{N-1}, \qquad (25)$$

and substituting in equation (23), we get

$$\mathbf{P}_N = [C_N][C_{N-1}]^{-1}\mathbf{P}_{N-1}. \qquad (26)$$

Equation (26) is the exit boundary condition we use to complete the definition of the boundary-value problem. Note

Copyright © 2001 by ASME

that (26) is not local, i.e., the density at the point $\rho'(N, i_o, j_o)$ depends on the value of density at all the grid points of the previous cross section $(N-1, i, j)$.

The formulation of the inflow condition will be similar to that of the exit condition except that the density associated with incoming acoustic waves will be subtracted from the total density prior to the application of the inflow conditions.

Once the pressure or density is determined, the velocity components can be calculated using the governing equations.

The inversion of the matrix $[C_{N-1}]$ in equation (26) could be difficult if acoustic modes with very large azimuthal number, m, are included in the expansion of equation (22). Such modes correspond to eigenvalues of very large imaginary part leading to elements of very small values in entire rows of the matrix $[C_{N-1}]$ causing the matrix to be ill-conditioned. The solution to this problem is to include only modes with eigenvalues which do not have large imaginary parts or do not decay quickly. As a result the number of modes used in the expansion may be less than the number of grid points (say n_p) at the $N-1$ axial location. However, a number of grid points equal to the number of modes (say n_m) have to be used in the formulation. The dimensions of the matrix $[C_{N-1}]$ in this case will be $n_m \times n_m$, and the dimensions of the matrix $[C_N]$ will be $n_p \times n_m$. The length of the vector $\mathbf{P}_N$ will be n_p and the length of the vector $\mathbf{P}_{N-1}$ will be n_m. The grid points to be included in $\mathbf{P}_{N-1}$ must be chosen carefully to obtain a matrix $[C_{N-1}]$ with good condition number. We choose these points such that the number of points taken in the radial direction equals the number of the n radial modes and the number of points in the circumferential direction equals the number of m circumferential modes. The chosen points should cover the whole cross section.

Results

Two sets of results are presented. In the first set, we consider the propagation of acoustic disturbances in a nonuniform swirling flow in an annular duct. We impose an arbitrary disturbance at the duct inlet and a nonreflecting boundary condition at the duct exit. The imposed disturbance upstream can be obtained from data or computations and satisfy the Euler equations. In the second set of results, we consider the problem of a gust interacting with an annular cascade producing unsteady lift on the blades and radiating sound in the farfield.

Sound Propagation in Swirling Flows

For the sake of comparison with known solutions, in this paper we impose an upstream disturbance in the form of a combination of the duct acoustic normal modes. The normal mode solution is of the form

$$\{\mathbf{u}, \rho'\}(x, \theta, r) = \{\mathbf{u}_{mn}, P_{mn}\}(r) e^{i(k_{mn}x + m\theta)}, \qquad (27)$$

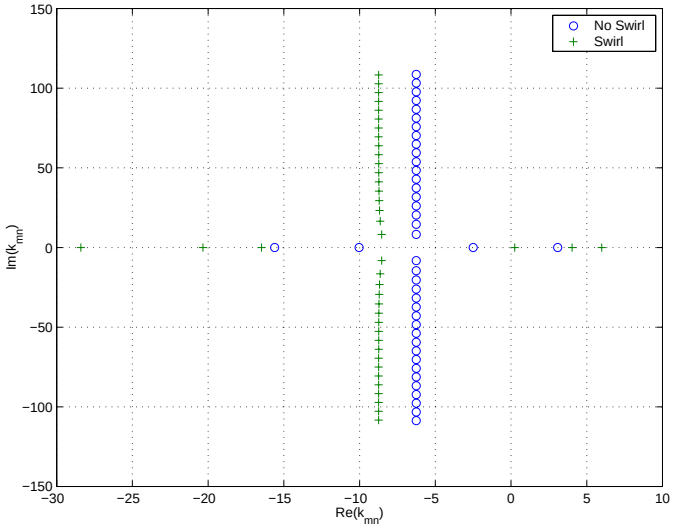

Figure 2. Acoustic eigenmodes spectra for uniform flow ($M_o = 0.5$), and swirling flow ($M_o = 0.5$, $M_\Omega = 0.2$ and $M_\Gamma = 0.2$) for a reduced frequency, $\omega = 9.3960$ and an azimuthal number, $m = -8$.

where n and m are the radial and circumferential modal numbers, respectively, and k_{mn} is the axial wave number. The corresponding velocity and density eigenfunctions of the mode (mn) are, $\mathbf{u}_{mn}$, and $P_{mn}(r)$, respectively.

A computational domain of angle $\frac{2\pi}{24}$, length r_m, and hub to tip ratio of 0.5 is considered. This geometry simulates the acoustic propagation downstream a stator of 24 vanes due to the interaction with the wakes of a 16 blades rotor located before the stator. The azimuthal numbers of the acoustic modes involved in the nonreflecting boundary conditions for this geometry will be very large if we consider a number of modes equal to the total number of grid points. To avoid the difficulties in inverting the matrix we limit the number of acoustic modes involved in the formulation to modes which have eigenvalues, k_{mn}, of imaginary parts less than 20.

Figure 2 shows the spectra of the acoustic eigenmodes k_{mn} for a uniform flow with an axial velocity $M_o = 0.5$ and a swirling flow defined by $M_o = 0.5$, $M_\Omega = 0.2$ and $M_\Gamma = 0.2$, for a circumferential wave number $m = -8$ and a reduced frequency of 9.396. The uniform flow has two downstream propagating modes ($k_{-8,1} = 3.0783$) and ($k_{-8,2} = -2.4965$) while the swirling flow has three downstream propagating modes ($k_{-8,1} = 5.9860$), ($k_{-8,2} = 4.0319$), and ($k_{-8,3} = 0.2416$).

We consider a combination of the three propagating acoustic modes of the swirling flow imposed at the inlet of the duct. The three modes will have the same weight. In other words, the coefficient of each mode imposed at the inlet of the duct is the same and we take them to be equal to 1.0. The nonreflecting boundary condition is applied at the duct exit. A uniform grid of 41 points

Copyright © 2001 by ASME

in the radial direction, 25 points in the circumferential direction and 65 points in the streamlines direction is used.

Figures 3-a, 3-b, and 3-c show the distribution of the flow variables as a function of x, θ, and r, respectively, plotted at $r = 1$ and $\theta = \theta_m = \pi/24$ for the axial variations, $x = 0.5$ and $r = 1$ for the circumferential variations, and $x = 0.5$ and $\theta = \theta_m$ for the radial variations. The figures show an excellent agreement between the numerical solution and the one obtained using the normal mode analysis. No reflections can be seen at the exit boundary. The coefficients of the acoustic modes are recalculated at the exit of the duct to estimate the dissipation due to numerical calculations. The coefficient at the duct exit for the first, second, and third modes are 0.9700, 0.9902, and 1.0188, respectively, indicating small dissipation error due to the numerical scheme.

For the above case of swirling flow the number of acoustic modes involved in the formulation of the outflow nonreflecting boundary condition is limited to the modes which have eigenvalues, k_{mn}, of imaginary parts less than 20. For this swirling flow, reduced frequency, and geometry, only three azimuthal numbers m satisfy this criterion. The three harmonics are 16, -8, and -32. The harmonic $m = -8$ has 5 radial modes of imaginary parts less than 20. The other harmonics have fewer number of radial modes of imaginary parts less than 20. In the boundary condition formulation 15 modes will be considered, 5 radial modes of each harmonic. In choosing the grid points involved in the formulation we consider 3 points in the circumferential direction (the same number of circumferential harmonics) and 5 points in the radial direction (the same number of radial modes). These 15 grid points should spread out over the cross section as much as possible.

Scattering of a Gust by a Row of Blades

In this section, we place a cascade of blades aligned with the streamlines in the middle third of the computational domain and apply our numerical algorithm to wake/blade row interaction. The computational domain which follows the streamlines will be the annular sector between two blades. A permeability condition will be imposed along the blade surfaces, i.e. the normal velocity component vanishes. A quasi-periodic boundary condition is applied along the circumferential boundaries before the blades for all the primitive variables. The quasi-periodic condition is applied for the pressure and the normal velocity only at the circumferential boundaries along the blade's wake. To validate our numerical scheme we consider the case proposed by Hanson [9] as a CAA Benchmark Problem from the 3rd Computational Aeroacoustic Workshop (Cleveland, Ohio, Nov 8-10 1999). In this problem, an annular cascade of 24 flat plate stator vanes is placed in a parallel annulus duct.The mean flow is axial and uniform. Analytically defined gust is introduced at the inlet of the duct. The gust is of the form,

$$\mathbf{v}(r,\theta,x,t) = \mathbf{a}(r)e^{i(pB\Omega x/U + pB\theta + 2\pi nq(r-r_h)/(r_t-r_h) - pB\Omega t)} \quad (28)$$

where U is the axial flow speed, Ω is the rotor (and Wake) angular velocity, and $B = 16$ is the number of rotor blades. We will consider the blade passing frequency (BPF) fundamental, $p = 1$, with upwash amplitude, $a_\theta = 0.1$. Reduced frequency $\omega b/U = pB\Omega b/U$ is constant over the span and equals to 6.5597, which corresponds to a tip Mach number $M_T = 0.783$, where b is the chord length and the hub-tip ratio is 0.5. We consider four cases with different wake phase variations, $q = 0$, 1, 2, and 3. Comparison is made with the existing lifting surface results of Namba [10] and Schulten [11] which are based on integral equation formulations of the problem.

Aerodynamics

In this subsection, we compare the aerodynamic results obtained from Schulten's lifting surface code against our numerical scheme for several cases with significant radial phase variations, $q = 1,3$, in the vortical disturbance. Figure(4) shows the real and imaginary parts of the unsteady pressure jump along the blade chord for $q = 1$ at different spanwise locations (%10, %50, and %90 span). The results are in good agreement with those obtained by Schulten. Figure(5) shows the real and imaginary parts of the unsteady pressure jump across the blade span for $q = 1$ at different chordwise locations (%10, %20, %50, and %90 chord). The results agree well with Schulten's results. Slight differences exist at the hub and the tip. Note the unsteady pressure jump shows significant variation from the hub to the tip.

Figure(6) shows the real and imaginary parts of the unsteady pressure jump across the blade span for $q = 3$ at different chordwise locations (%10, %20, %50, and %90 chord). The radial variations for $q = 3$ are significant. The radial variations increase as we get closer to the leading edge. Again, the results agree well with Schulten's results. Slight differences exist at the hub and the tip.

Acoustics

In this subsection, the acoustic amplitudes at the inflow/outflow boundaries are obtained using the eigenfunction expansion (21). To present acoustic results, the complex coefficients C_{mn} defined by (21) will be compared to those obtained by Namba and Sculten for the upstream and downstream propagating modes where m here is the azimuthal order of the modes, $B - mV$ defined by Taylor and Sofrin [12] and n is the radial order of the mode which represents the number of the zero crossings in the radial direction of the eigenfunction P_{mn}. The axial wave number, k_{mn}, is real if the mode is propagating and complex if the mode is decaying.

Copyright © 2001 by ASME

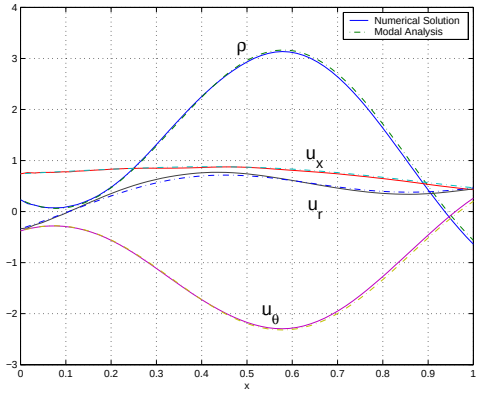

a) Axial distribution of flow quantities.

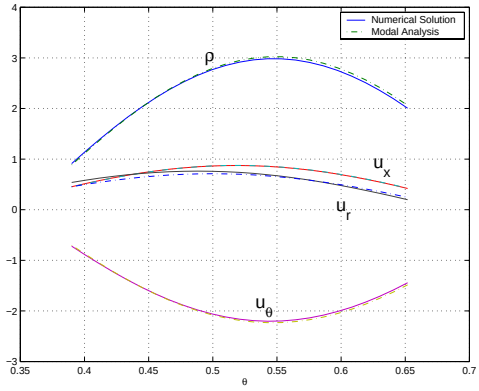

b) Circumferential distribution of flow quantities.

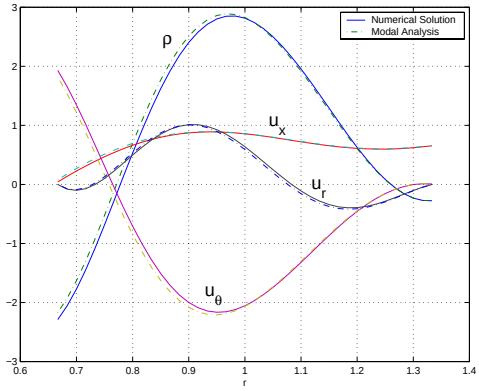

c) Radial distribution of flow quantities.

Figure 3. A combination of the three propagating acoustic modes in a swirling flow $M_o = 0.5$, $M_\Omega = 0.2$ and $M_\Gamma = 0.2$ for a reduced frequency, $\omega = 9.3960$, an azimuthal number, $m = -8$, and a grid of ($n_r \times n_\theta \times n_x = 41 \times 25 \times 65$).

The normal mode spectrum of Fig. (2) shows that for these parameters there are two propagating modes upstream and two propagating modes downstream. They correspond to modes (1,0) ($m = 1, n = 0$),and (1,1).

Figure(7) shows the real and imaginary parts of the coefficient C_{10} upstream and downstream. The computed values are compared to those of Namba and Sculten for $q = 0, 1, 2$, and 3. Overall, the computed values are closer to Schulten, especially for $q = 1$. The three results are almost identical for $q = 2$ and 3. The coefficient, C_{11}, of the second propagating mode show Similar behavior as can be seen in Fig.(8).

The absolute values of the coefficients C_{10} and C_{11} are

Copyright © 2001 by ASME

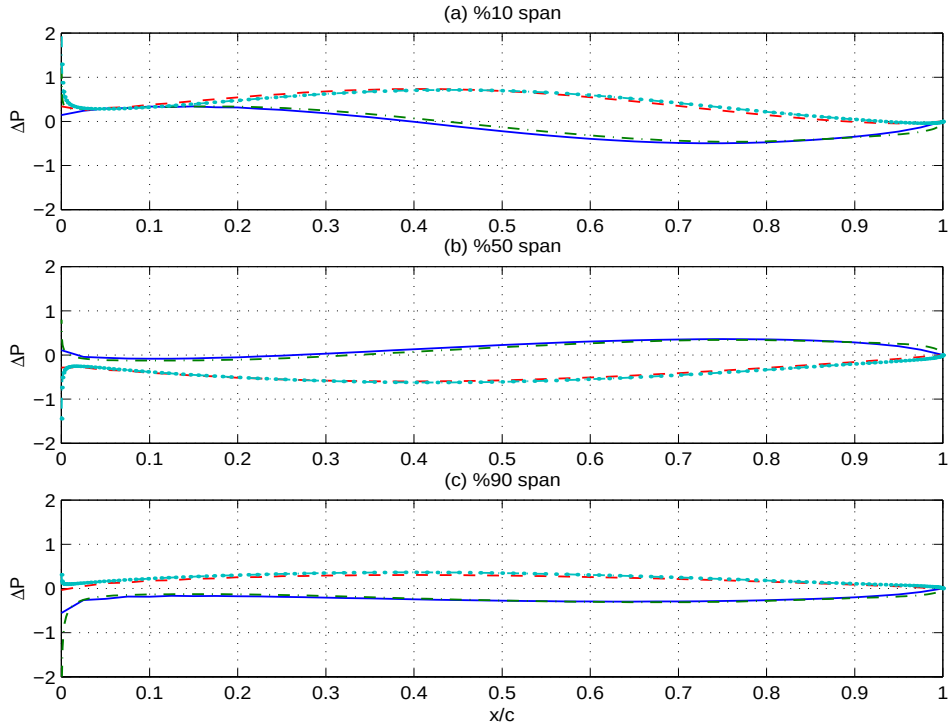

Figure 4. Unsteady pressure jump along the blade chord for $q = 1$ at different spanwise locations. Current computations (real part (-), imaginary part(- -)) are compared to those of Schulten (real part (-.-), imaginary part (..))

shown in table (1) for the upstream propagating modes and in table (2) for the downstream propagating modes.

Comparison to Strip Theory

For broadband applications one must determine an acoustic response spectrum which requires solving the gust response problem for many frequencies and spinning mode orders. Due to the computational intensiveness of solving the three-dimensional gust response problem, strip theory is used for both the aerodynamics and the acoustic propagation [5]. In the strip theory, solutions are obtained at specific radii. At each radius, the solution is obtained by assuming the radius is infinite, reducing the problem to a two dimensional one. This process is repeated for a finite number of radii. In this section, we compare our computations to the strip theory to see the extent to which the strip theory approximation is adequate for real three dimensional geometries.

Figure (9) shows the distribution of the absolute value of the unsteady lift coefficient normalized by $\pi\rho_o a_\theta U b$ across the span. Our three dimensional computations are compared to the strip theory approximation obtained using a two dimensional integral formulation [8]. The figure shows poor comparison especially near the hub radius where the two dimensional solution shows an abrupt drop in the value of the unsteady lift coefficient. In addition, the two dimensional acoustic calculations show that only one mode is cut on corresponding to $m = 1$. This mode cuts on for $r > 0.74$. This explains the abrupt decrease in the lift coefficient at $r = 0.74$ which corresponds to 10% span.

The three dimensional calculations showed that there are two propagating radial modes $n = 0, 1$ of $m = 1$. Since the strip theory is a two-dimensional theory with no dependence on the radius, it does not predict the two radial modes of the three-dimensional calculations. In order to compare the three dimensional acoustic calculations to the strip theory approximation, we calculate the pressure due to the two propagating modes of the three dimensional calculations and compare it to the acoustic pressure of the strip theory single mode. Figure (10) shows this comparison upstream and downstream. Again, the comparison is poor for the upstream acoustics and for the downstream acoustics near the hub and the tip.

Conclusions

Inflow/outflow conditions are implemented in a linearized 3-D Euler equations scheme to study the generation and propagation of acoustic disturbances in a nonuniform swirling mean flow in an annular duct. The numerical solutions of acoustic waves propagating in a swirling flow are validated by comparison with a normal mode analysis. The scattering problem of a gust interacting with an annular cascade is studied. The solutions are

Copyright © 2001 by ASME

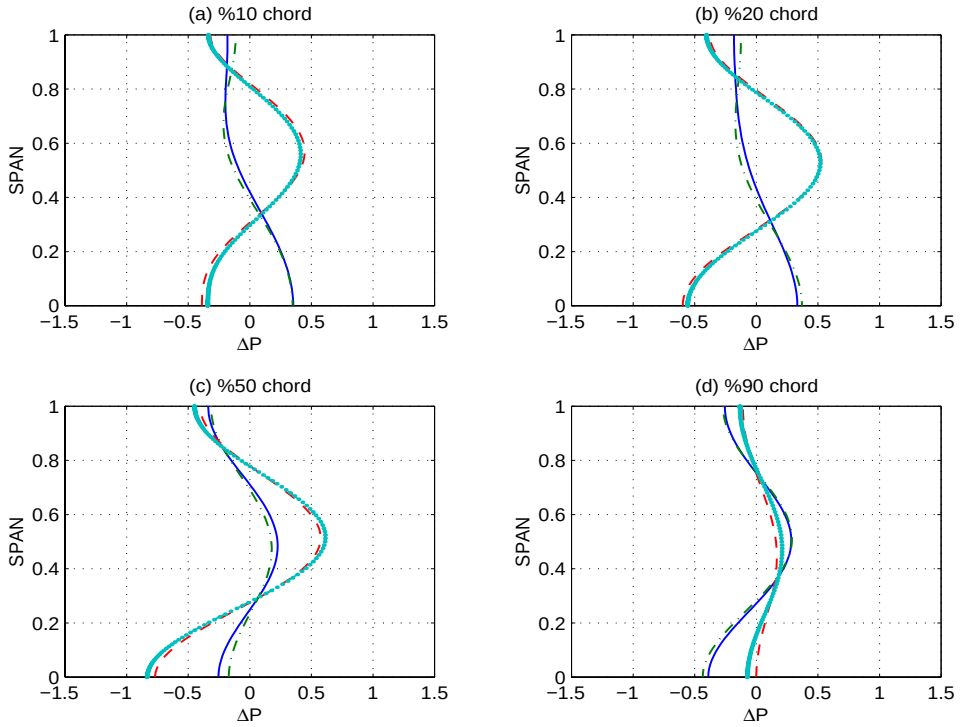

Figure 5. Unsteady pressure jump along the blade span for $q = 1$ at different chordwise locations. Current computations (real part (-), imaginary part(- -)) are compared to those of Schulten (real part (-.-), imaginary part (..))

q	m	μ	Namba	Sculten	Current Computations
0	1	0	1.1780×10^{-2}	1.1745×10^{-2}	1.3332×10^{-2}
0	1	1	1.9301×10^{-2}	1.9064×10^{-2}	1.8358×10^{-2}
1	1	0	1.6870×10^{-3}	4.1793×10^{-3}	3.9596×10^{-3}
1	1	1	1.3088×10^{-2}	2.2913×10^{-2}	2.0612×10^{-2}
2	1	0	8.9005×10^{-4}	9.4530×10^{-4}	1.0867×10^{-3}
2	1	1	4.8305×10^{-3}	3.8368×10^{-3}	4.4787×10^{-3}
3	1	0	5.8400×10^{-4}	6.5845×10^{-4}	7.1097×10^{-4}
3	1	1	3.0332×10^{-3}	2.6001×10^{-3}	2.9529×10^{-3}

Table 1. Absolute values of the upstream coefficients C_{mn}

validated by comparison with the semi-analytic solutions of the lifting surface methods. The solutions are also compared to the strip theory approximation. The comparison showed that strip theory is not a good approximation in predicting the unsteady aerodynamics and the acoustics of the three dimensional scattering problem.

Acknowledgments

This research is partially supported by United Technologies Pratt & Whitney under NASA Glenn AST NAS 3-27727 with Dennis Huff as project manager. Thanks to professor Schulten for providing us aerodynamic results to compare our solutions with.

Copyright © 2001 by ASME

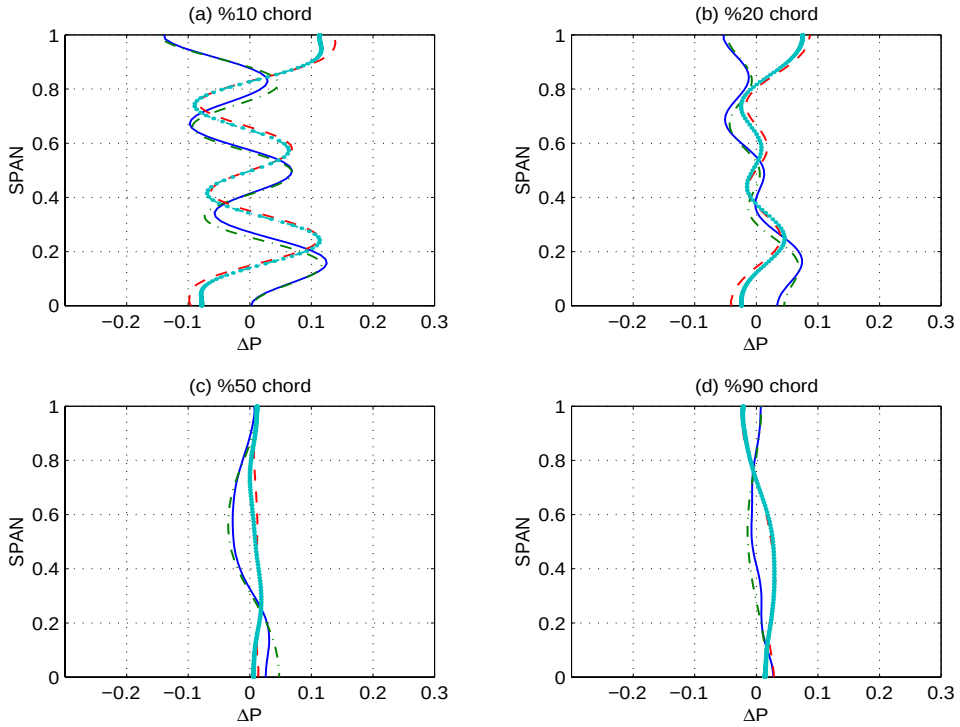

Figure 6. Unsteady pressure jump along the blade span for $q = 3$ at different chordwise locations. Current computations (real part (-), imaginary part(- -)) are compared to those of Schulten (real part (-.-), imaginary part (..))

q	m	μ	Namba	Sculten	Current Computations
0	1	0	1.7144×10^{-2}	1.4972×10^{-2}	1.8328×10^{-2}
0	1	1	1.8946×10^{-2}	1.7850×10^{-2}	1.8413×10^{-2}
1	1	0	1.0155×10^{-2}	9.9075×10^{-3}	1.0863×10^{-2}
1	1	1	2.7500×10^{-2}	2.4696×10^{-2}	2.5465×10^{-2}
2	1	0	3.3653×10^{-3}	3.0988×10^{-3}	3.6577×10^{-3}
2	1	1	6.0722×10^{-3}	6.6977×10^{-3}	6.1183×10^{-3}
3	1	0	2.0496×10^{-3}	1.9710×10^{-3}	2.3436×10^{-3}
3	1	1	3.7287×10^{-3}	4.2455×10^{-3}	3.9937×10^{-3}

Table 2. Absolute values of the downstream coefficients C_{mn}

References

[1] A. A. Ali, O. V. Atassi, and H. M. Atassi. Acoustic eigenmodes in a coannular duct with a general swirling flow. In *AIAA 2000-1954, 6th AIAA/CEAS Aeroacoustics Conference at Maui,Hawai*, 2000.

[2] O. V. Atassi. Inflow/outflow conditions for time-harmonic internal aeroacoustic problems. In *AIAA 99-0482, 37th AIAA aerospace sciences meeting and exhibit, Jan. 11-14, Reno, NV*, 1999.

[3] J. Fang and H.M. Atassi. *Compressible Flows with Vortical Disturbances Around a Cascade of Loaded Airfoils. In Unsteady Aerodynamics, Aeroacoustics, and Aeroelasticity of Turbomachines and Propellers*, pages 149–176. Ed. Atassi, H. M., 1993. Springer-Verlag.

Copyright © 2001 by ASME

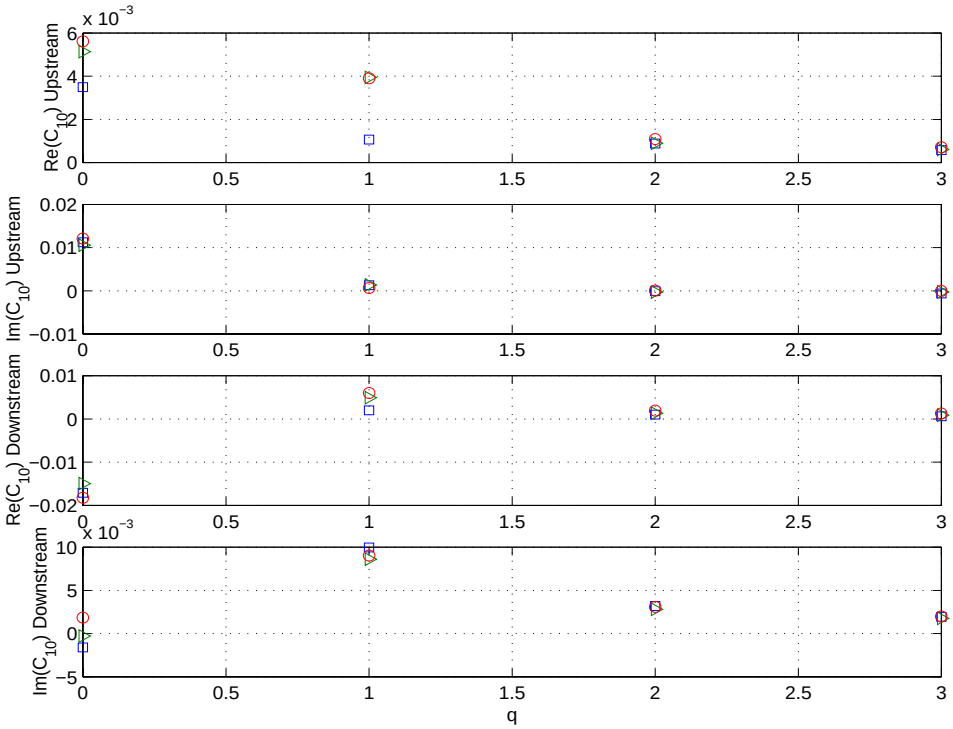

Figure 7. Complex Acoustic amplitudes, C_{10} of the propagating mode (1,0) upstream and downstream for different values of the wake phase parameter, q. Current computations (○), are compared to those of Namba (□) and Schulten (▷)

[4] M. B. Giles. Nonreflecting boundary conditions for Euler equation calculations. *AIAA Journal*, 28(12):2050–2058, 1990.

[5] S. Glegg and N. Walker. Fan noise from blades moving through boundary layer turbulence. In *Fifth AIAA/CEAS Aeroacoustics Conference*, 1999.

[6] V. V. Golubev and H. M. Atassi. Acoustic-vorticity waves in swirling flows. *Journal of Sound and Vibration*, 209(2):203–222, 1998.

[7] V. V. Golubev and H. M. Atassi. Unsteady swirling flows in annular cascades. part I. evolution of incident disturbances. *AIAA*, 38:1142–1149, 2000.

[8] G. Hamad and H. M. Atassi. Sound generation in a cascade by 3D disturbance convected in a subsonic flow. In *AIAA 81-2046, 7th Aeroacoustic Conference, Palo Alto, CA*, 1981.

[9] D. B. Hanson. Fan stator with harmonic excitation by rotor wake, 1999. Third CAA Workshop on Benchmark Problems, Category 4.

[10] M. Namba. Three-dimensional analysis of blade force and sound generation for an annular cascade in distorted flows. *Journal of Sound and Vibration*, 50:479–508, 1977.

[11] J. B. H. M. Schulten. Sound generated by rotor wakes interacting with a leaned vane stator. *AIAA Journal*, 20:1352–1358, 1982.

[12] J. M. Tayler and T. G. Sofrin. Axial flow compressor noise studies. *SAE Transactions*, 70:309–332, 1962.

[13] R. Vichnevetsky and E. C. Parsier. Non-reflecting upwind boundaries for hyperbolic equations. *Numerical Methods for Partial Differential Equations*, 2(1):1–12, 1986.

[14] F.R.S. whitham. *Linear and Nonlinear Waves*. John Wiley & Sons, 1974.

Copyright © 2001 by ASME

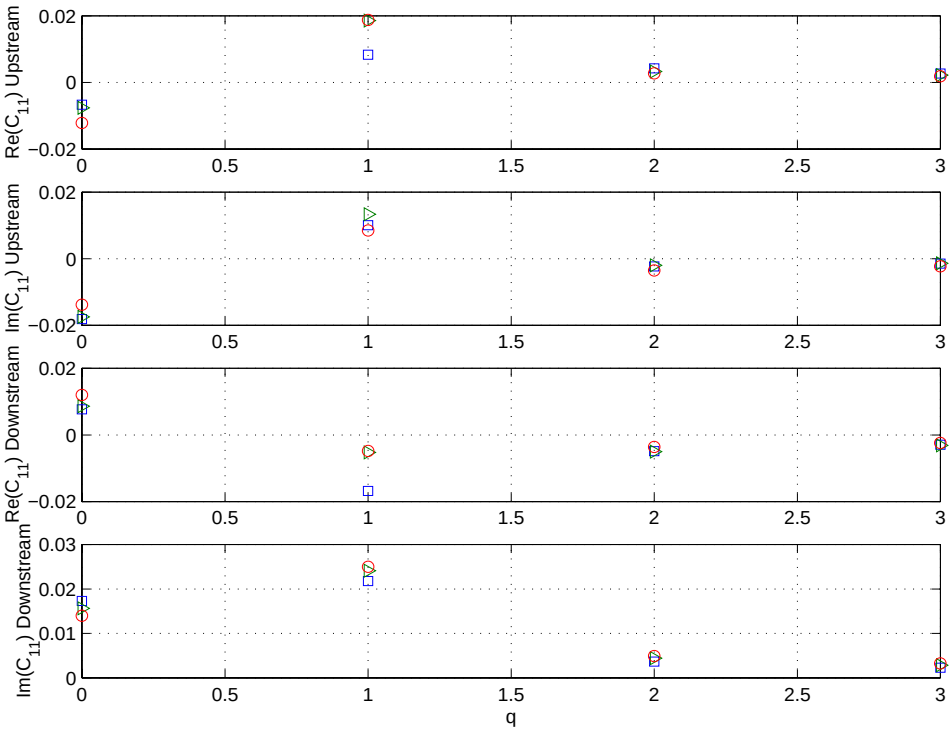

Figure 8. Complex Acoustic amplitudes, C_{11} of the propagating mode (1,1) upstream and downstream for different values of the wake phase parameter, q. Current computations (○), are compared to those of Namba (□) and Schulten (▷)

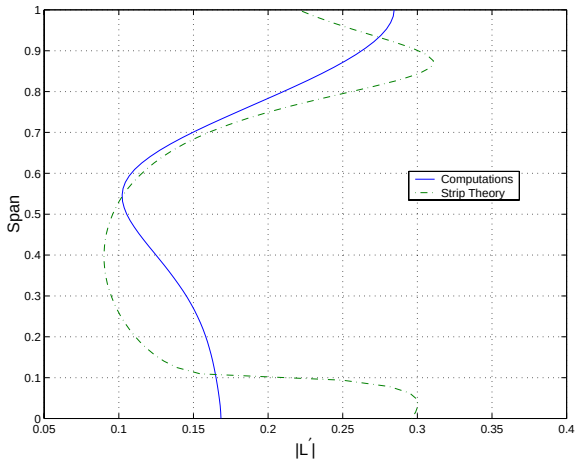

Figure 9. A comparison between the unsteady lift of the three dimensional computations and the strip theory approximation for a uniform flow and $q = 0$.

Copyright © 2001 by ASME

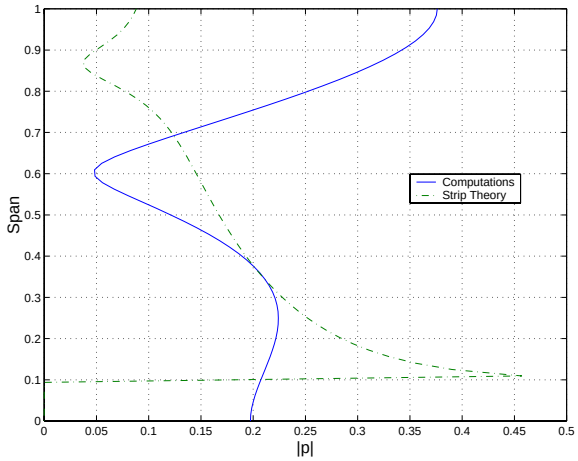

a) Upstream Acoustics

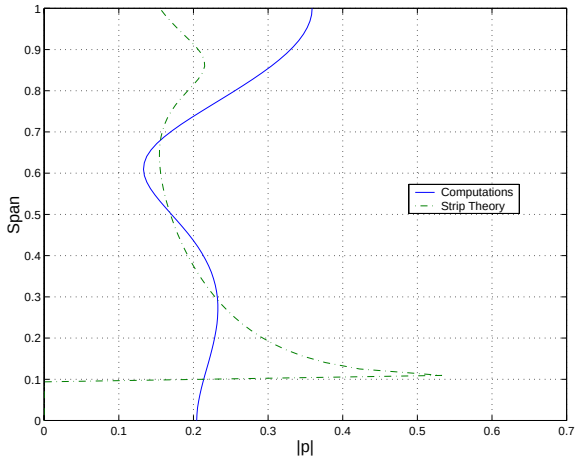

b) Downstream Acoustics

Figure 10. A comparison between the acoustics of the three dimensional computations and the strip theory approximation for a uniform flow and $q = 0$.

Copyright © 2001 by ASME